Ming Hao
Department of Mechanical Engineering,
Tsinghua University,
Beijing 100084, China
e-mail: haom16@mails.tsinghua.edu.cn

Jiwen Zhang
Department of Mechanical Engineering,
Tsinghua University,
Beijing 100084, China
e-mail: jwzhang@mail.tsinghua.edu.cn

Ken Chen
Department of Mechanical Engineering,
Tsinghua University,
Beijing 100084, China
e-mail: kenchen@tsinghua.edu.cn

Harry Asada
Department of Mechanical Engineering,
Massachusetts Institute of Technology,
Cambridge, MA 02139
e-mail: asada@mit.edu

Chenglong Fu[1]
Department of Mechanical and
Energy Engineering,
Southern University of Science and Technology,
Shenzhen 518055, China
e-mail: fucl@sustech.edu.cn

Supernumerary Robotic Limbs to Assist Human Walking With Load Carriage

Walking with load carriage is a common requirement for individuals in many situations. Legged exoskeletons can transfer the load weight to the ground with rigid-leg structures, thus reducing the load weight borne by the human user. However, the inertia of paralleled structures and the mechanical joint tend to disturb natural motions of human limbs, leading to high-energy consumption. Different from exoskeletons, Supernumerary Robotic Limbs (SuperLimbs) are kinematically independent of the human limbs, thus avoiding the physical interference with the human limbs. In this paper, a SuperLimb system is proposed to assist the human walking with load carriage. The system has two rigid robotic limbs, and each robotic limb has four degrees-of-freedom (DOFs). The SuperLimbs can transfer the load weight to the ground through the rigid structures, thus reducing the weight borne by the human user. A hybrid control strategy is presented to assist the human as well as avoid disturbing user's natural motions. Motions of the SuperLimb system are generated autonomously to follow the gait of the human user. The gait synchronization is controlled by a finite state machine, which uses inertial sensors to detect the human gait. Human walking experiments are conducted to verify this concept. Experiments indicate that the SuperLimbs can follow the human gait as well as distribute the load weight. Results show that our SuperLimb system can reduce 85.7% of load weight borne by the human when both robotic limbs support and 55.8% load weight on average. This study may inspire the design of other wearable robots and may provide efficient solutions for human loaded walking. [DOI: 10.1115/1.4047729]

Keywords: supernumerary robotic limbs, superlimbs, wearable robot, biped locomotion, human loaded walking, multi-body dynamics and exoskelotons, prosthetics

1 Introduction

Walking with load carriage is a common requirement for individuals in occupational and military activities. Firefighters and other emergency workers use backpacks to carry equipment such as Self-Contained Breathing Apparatuses (SCBA) [1]. Infantry soldiers often carry heavy carriages and walk long distances. Wearable robots such as exoskeletons can benefit people who engage in load carrying. Lower-extremity exoskeletons have been developed for several decades to enhance and assist human locomotion, increasing the load capacity of users. Legged exoskeletons can transfer the load weight to the ground by supporting the carriage [2–4]. Joint-level exoskeletons can apply assistive torques to the joints, thus lowering the energy consumption of users in carrying loads [5,6].

Although exoskeletons can benefit people in walking with carriages, some technological challenges are faced. According to structures, lower-extremity exoskeletons can be divided into two categories: legged exoskeletons and joint-level exoskeletons. Legged exoskeletons usually have rigid-leg structures paralleled with human limbs to support carriages [2–4]. Leg structures can transfer the load weight to the ground, thus reducing the weight borne by the human user. However, the inertia and joints of rigid legs tend to disturb natural motions of human limbs, which leads to substantial extra energy consumption [5,7,8]. Joint-level exoskeletons only have structures fixed on target joints [5–7,9–11], which can not support the load weight. To assist human walking with load carriage, new mechanisms are needed to reduce the load weight borne by the user, as well as avoid the physical interference with human limbs.

A novel form of wearable robot, Supernumerary Robotic Limbs (SuperLimbs), was proposed in recent years [12–27]. Different from exoskeletons, structures of SuperLimbs are kinematically independent of the human limbs. Thus, SuperLimbs can avoid physical interference problems of legged exoskeletons and provide extra support without constraining human limbs [22]. Current researches on SuperLimbs include grasping or supporting objects [12–16], supporting body [17–22], sitting/standing assistance [23], and assisting stance transition [24,25]. Parietti et al. proposed a SuperLimb system to support the human body when the human worked in uncomfortable poses [22] and augment the balance by increasing the area of the support polygon [21]. Treers et al. demonstrated a SuperLimb prototype that could provide assistant force in sitting/standing motions [23]. Gonzalez and Asada designed a SuperLimb system that can assist human both in standing and crawling configurations [24,25]. To control SuperLimbs, different control methods were proposed including Inertial Measurement Units (IMU) control [16], EMG control [26], and Brain–Machine Interface (BMI) control [27]. These methods use wearable sensors to recognize user's commands to control SuperLimbs.

Because of the independent structures, SuperLimbs are applicable to assist the human walking with load carriage. They can use rigid structures to distribute the load weight as well as avoid disturbing natural motions of human limbs. However, to our knowledge, no SuperLimb system has been demonstrated to assist human loaded walking practically. Human walking is complex and rhythmic, involving the coordination of the brain, nerves, and muscles to generate the force necessary for locomotion [28,29]. Both the mechanical design and the control strategy are technically challenging in this task. First, the SuperLimbs should have enough power to assist the human user: output support force to support the load

[1]Corresponding author.

Contributed by the Mechanisms and Robotics Committee of ASME for publication in the Journal of Mechanisms and Robotics. Manuscript received December 30, 2019; final manuscript received June 15, 2020; published online July 28, 2020. Assoc. Editor: Panagiotis Artemiadis.

weight and have enough speed to follow the user's gait. Second, the SuperLimbs should generate motions autonomously without conscious commands from the human user, to avoid disturbing the natural rhythm of walking.

In this paper, a SuperLimb system to assist human loaded walking is proposed, as Fig. 1 shows. The system has two rigid robotic limbs, and each robotic limb has four degrees-of-freedom (DOFs). The SuperLimbs can transfer the load weight to the ground through the rigid structures, thus reducing the weight borne by the human user. A hybrid control strategy is presented to avoid disturbing the user's natural motions. Motions of the SuperLimbs are generated autonomously to follow the gait of the human user. The gait synchronization is realized by a finite state machine, which uses foot-worn IMUs to measure the human gait. Walking experiments are conducted to provide an initial proof of this concept. Experiments indicate that the SuperLimb system can follow the human gait as well as distribute the load weight. Compared with the normal backpack, the SuperLimbs can reduce 85.7% load weight borne by the human when both robotic limbs support, and 55.8% load weight on average.

In the following content, Sec. 2 introduces the mechanical design of the SuperLimb system. Section 3 focuses on the gait synthesis with the sensory control. The human walking experiment is conducted to verify the concept in Sec. 4. Section 5 provides a summary of this work and the outline of our plan in the future.

2 Mechanical Design

The mechanical design of the SuperLimb system is shown in Fig. 2. The system consists of two robotic limbs and a backpack base. The SuperLimb system bears the payload and transfers the weight to the ground through the robotic limbs, thus reducing the weight borne by the human user. Each robotic limb has four DOFs: two rotational DOFs at the hip joint, one prismatic joint, and one rotational DOF at the knee joint, as Fig. 2(*a*) shows. As the primary objective of this SuperLimb system is to assist human loaded walking, two functions are required for each robotic limb: support the weight to reduce the load borne by the user and swing to next stride to follow the human gait. Two rotational DOFs at the hip as well as the prismatic joint allows the endpoint of the robotic limb to reach an arbitrary position in space. The knee joint can flex the robotic limb when the limb swings to the next stride and can be locked when the limb supports the load weight.

Fig. 1 Photos of the SuperLimb system worn by a participant: (*a*) side view and (*b*) axonometric view. The SuperLimb system contains two robotic limbs, which can distribute the carriage weight through the structure, thus reducing the weight borne by the participant. The robotic limbs are kinematically independent of the participant's limbs, avoiding the physical interference with the human limbs.

The side view of the backpack base design is shown in Fig. 2(*b*). The backpack base consists of two main parts: the backpack and the robot base, connecting each other with a force sensor and linear slides. The robot base connected with two robotic limbs bears the payload, and the backpack is worn by the human user. Thus, the force sensor can measure the vertical interaction force between the human user and the SuperLimbs, which approximately equals the weight borne by the user. The objective of this design is to evaluate the performance of the SuperLimbs in Sec. 4.3.

Two rotational DOFs of the hip joint, actuated by Dynamixel MX-64 (8.4 Nm, 165 g) and MX-106 (6 Nm, 165 g), intersect, forming an equivalent ball-and-socket joint. The prismatic joint allows the robotic limb to extend and retract, transferring the load weight to the ground. As most of the load is borne in the longitudinal direction of each robotic limb, axial forces coming from the robotic limbs pass through the center of the equivalent ball-and-socket joint and do not generate any torque. Thus, most of the load weight is borne by the prismatic joint, and servomotors of the hip joint are only used when the robotic limb swings to the next stride.

As the prismatic joint needs to bear most of the load during human walking, the joint should be able to output sufficient force and move in moderate velocity. The detailed view of the prismatic joint is shown in Fig. 2(*c*). The linear movement is implemented by a belt and linear slide device. The torque of the motor (Maxon EC-4pole30, 16,500 rpm, 200 W) is first amplified by a gearhead (Maxon GP42C, reduction 4.3:1) fixed on the motor and is then amplified by two belt devices with a 2:1 reduction. Finally, the amplified torque actuates the linear movement of the prismatic joint toward the belt and linear slide device. We do not use the screw mechanism, because the high gear ratio of screw mechanism would limit the linear velocity of the prismatic joint. The theoretical maximum velocity of the prismatic joint can reach up to 104 cm/s. In the practice, the maximum velocity we used is 20 cm/s for safety, which can meet the requirement of following natural gait of the human.

The mechanical design of the knee joint is shown in Fig. 2(*d*). This joint has two basic functions: lock the joint when the robotic limb bears the load and flex the limb when the limb swings. The knee joint is implemented by a four-bar linkage actuated by a lightweight servomotor (Dynamixel MX-28, 2.5 Nm, 72 g). When the robotic limb contacts the ground, the servomotor rotates to the mechanical dead-point of the four-bar linkage, locking the joint with small torque. Thus, the load weight could be transferred on the ground through the locked joint. When the robotic limb is off the ground to swing to the next stride, the servomotor flexes the limb, preventing the endpoint of the limb from touching the ground. It should be noted that the retraction of the prismatic joint can realize a similar function in level ground walking. However, the range of the prismatic joint is not enough in stair climbing, which is one of our future plans. To extend the flexibility in different road conditions, the knee joint is designed with small additional mass.

Figure 2(*e*) shows the spring device at the end of the robotic limb. According to Hooke's law, the relationship between the force borne by the robotic limb F and the compression of the spring Δx is $F = k\Delta x$, where k is the stiffness of the spring. Thus, the control of F can be transformed into the control of Δx by adjusting the length of robotic limb, when the limb contacts the ground. Figure 3 shows the diagram of the force control.F^d is the desired force, and F^r is the real force measured by the force sensor at the end of robotic limb. Δx_p is the position error of the prismatic joint. The force

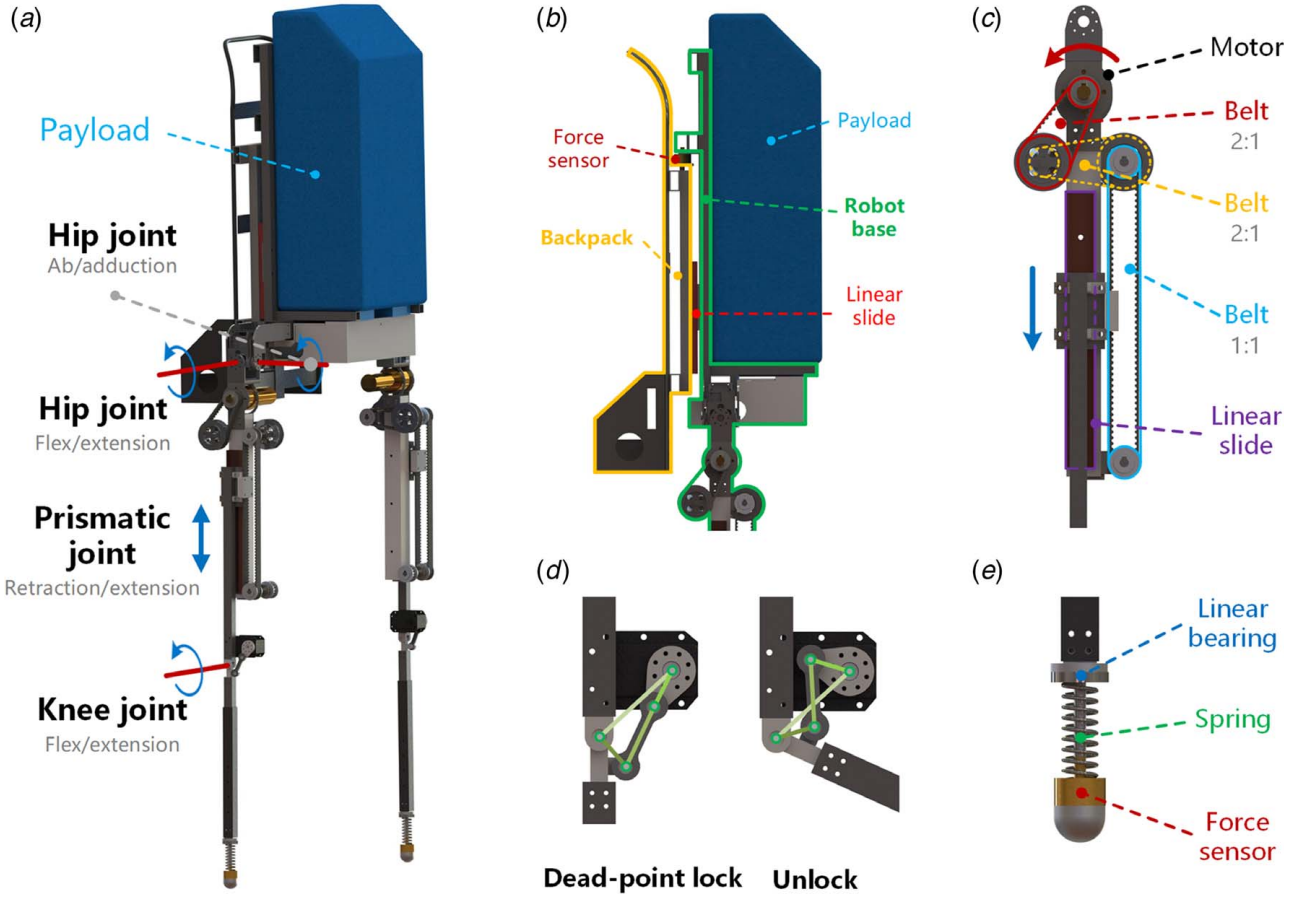

Fig. 2 3D model of the SuperLimb system. (*a*) DOFs of the SuperLimb system. The system contains two robotic limbs and a backpack base that bears the payload. Each robotic limb has four DOFs: two rotational DOFs at the hip joint, one prismatic joint and one rotational DOF at the knee joint. (*b*) Side view of the SuperLimb base. The load weight borne by the human can be measured by the force sensor, to evaluate the performance of the system. (*c*) View of the prismatic joint. The torque of the motor is first amplified by two belt devices with a 2:1 gear ratio and then actuates the linear motion of the slider towards the belt and linear slide device. (*d*) View of the knee joint. The lock state is implemented by the dead-point lock of the four-bar linkage, allowing the servomotor to lock the joint with small torque. (*e*) Detailed view of the spring device at the end of the robotic limb.

error ΔF is transformed into Δx_p with a PI controller, and then is fed into the position controller of the prismatic joint to adjust the length of robotic limb. The position controller is implemented by a PID controller by an Elmo controller (SOL-WHI10/60E03). The function of the force control is tested by experiments shown in Sec. 4.1.

To lower the weight of the system, the main frames use carbon fiber tubes, and connection structures use the sheet-metal. Other components of differential mechanisms are fabricated on the CNC mill, made of aluminum alloy. The weight of the SuperLimb system is 6.5 kg, including the structures, motors, and sensors.

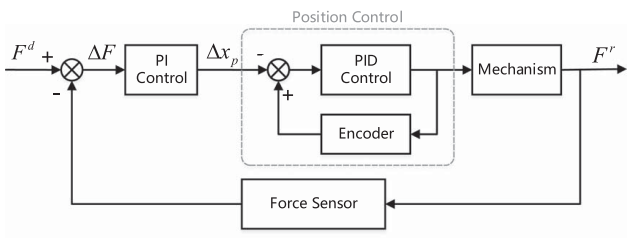

Fig. 3 Diagram of the force control of the prismatic joint. F^d is the desired force, and F^r is the real force measured by the force sensor at the end of robotic limb. The force error ΔF is transformed into the position error Δx_p and then fed into the position control of the prismatic joint.

The SuperLimb system is a self-contained system with the control box and the battery on itself, resulting in an additional weight of 2.2 kg.

3 Gait Control

Human walking is complex and rhythmic and involves the coordination of the brain, nerves, and several muscles [28,29]. To assist this task, on one hand, the SuperLimbs should output necessary forces to distribute the load weight borne by the human user and reduce unnecessary forces or torques that would constrain the human motions. On the other hand, the SuperLimbs should follow the walking rhythm and generate motions autonomously, which avoids disturbing the walking rhythm. To achieve these two targets, we first focus on the control strategy and then discuss the gait generation of the SuperLimbs corresponding with the gait of the human user. Finally, the gait synchronization is implemented by a finite state machine with an IMU-based sensory control.

Figure 4 shows the diagram of the control strategy. When the robotic limb is off the ground, position controls are used on all joints to let the robotic limb swing to the next stride, thus following the gait of the human user. When the robotic limb touches the ground, the hip joints are switched to zero-torque mode, behaving like a passive ball-and-socket joint. Most of the load weight is borne by the structure and the prismatic joint. The force control is used on the prismatic joint to let the limb retract and extend to follow the movement of the user's body, and a force is output

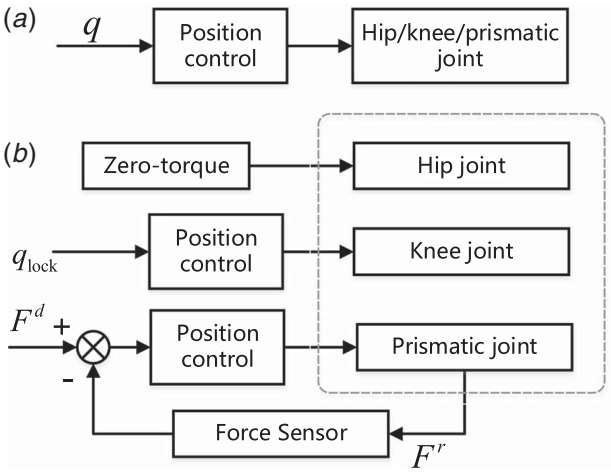

Fig. 4 Diagrams of the hybrid control strategy. (*a*) Position control strategy. Position controls are used on all joints of the robotic limb, to let the limb swing to the target configuration. (*b*) Force control strategy. When the robotic limb touches the ground, the hip joint is switched to the zero-torque mode, behaving as a passive joint. The knee joint is locked by the mechanical dead point of the four-bar linkage. The force control is used on the prismatic joint to distribute the load weight.

from the prismatic joint to support the load. The knee joint is locked to transfer the weight to the ground. By the coordination of the hip joint, the prismatic joint, and the knee joint, the robotic limb can distribute the weight borne by the user and avoid constraining the user's motion kinematically.

Figure 5 describes the gait cycle of the SuperLimbs. From the toe-off to the heel-strike, the human leg is in the swing phase, where the robotic limb works in the robotic-limb-swing mode. In this mode, the robotic limb swings forward to the next stride, by position control of the hip joint, the prismatic joint, and the knee joint. Motions of the joints over the human gait are illustrated in Fig. 5. Position trajectories of the joints are formulated by the cubic spline interpolation. When all joints arrive, the robotic limb will maintain the configuration and wait for the heel-strike of the human leg.

After the heel-strike, the human leg goes into the stance phase, and the robotic limb switches into the touch-down mode. In this mode, the robotic limb swings backward and extends its length, making the endpoint touching the ground. Once the robotic limb touches the ground, it switches into the robotic-limb-support mode. The hip joint is switched into the zero-torque mode, and the load weight is distributed by the prismatic joint whereby the force control method. When the human leg goes into the next swing phase, the mode is changed into the robotic-limb-swing mode again.

Gait phases of the two robotic limbs are shown in Fig. 6. Each robotic limb follows the gait of the human leg on the ipsilateral side. When the robotic limb works in the robotic-limb-support mode, it can transfer the load weight to the ground through the prismatic joint, thus reducing the weight borne by the human. When one robotic limb is in the robotic-limb-swing or the touch-down mode, the load weight is distributed by the other robotic limb, thus avoiding the human user bearing all the load.

To synchronize the gait of the SuperLimbs and the human user, an IMU-based sensory control method is proposed. The diagram of the sensory control is shown in Fig. 7. A finite state machine is used to control the work mode of the robotic limb. The work mode will be changed if the corresponding event, heel-strike, toe-off, and robotic-limb-contact, is detected. The event of the robotic-limb-contact will be detected if the output of the force sensory exceeds the force threshold. Events of the heel-strike and the toe-off are detected by the IMU worn on the user's heel. The heel-strike is detected with a threshold method on accelerometer outputs, and the toe-off is detected as the minimal negative peak of gyroscope outputs [30]. Besides the IMUs worn on the heel, a third IMU fixed on the SuperLimb base is used to measure the pitch angle of the base, compensating the sway of the user's body. It confirms that the robotic limb can reach the target configuration in the robotic-limb-swing mode.

4 Experiments

To verify the control method and the concept of SuperLimbs, several experiments are carried out in this section, including force control tests, walking tests, and load weight comparisons.

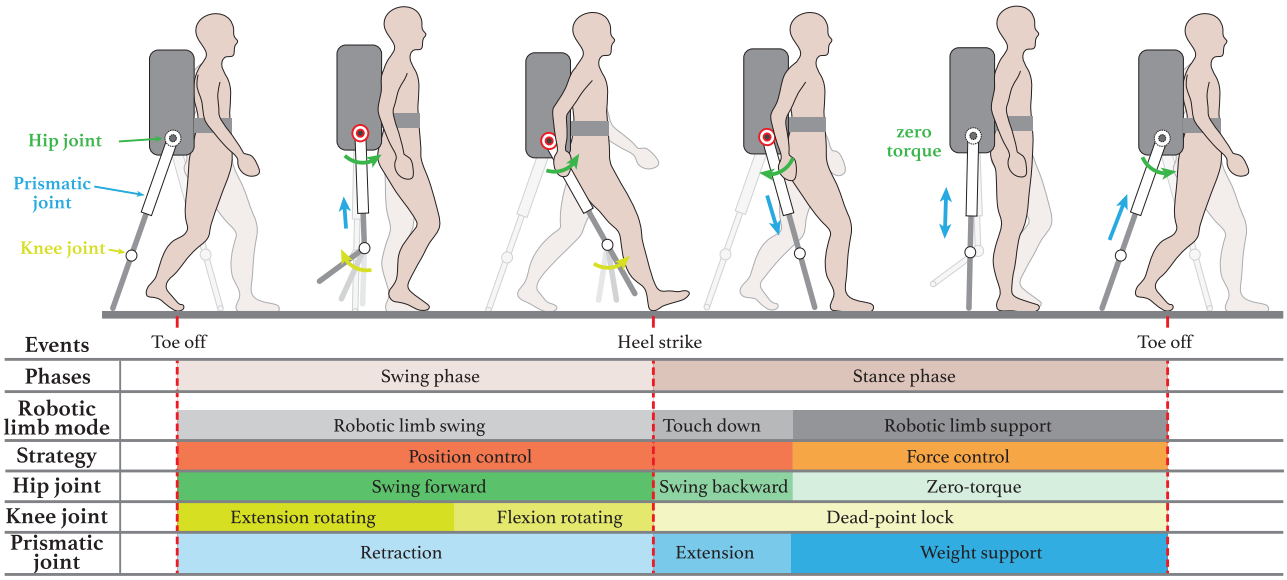

Fig. 5 Diagram of the SuperLimb gait cycle. During the swing phase of the human, the robotic-limb-swing mode is entered, where the position control strategy is used to let the robotic limb swing forward to the next stride. When the stance phase of the human begins, the robotic limb changes into the touch-down mode, touching the ground actively to enter the next mode. In the robotic-limb-support mode, the force control strategy is used to distribute the load weight borne by the human user.

4.1 Force Control Test of Prismatic Joint. To verify the function of the force control method on the prismatic joint, the force control test is conducted. In the test, the robot base is fixed still on a frame with the tested robotic limb touching the ground. Figure 8 shows the test result. The desired force F^d is designed in sinusoid or triangle form and is fed into the control loop shown in Fig. 3. The real force F^r is measured with the force sensor fixed at the end of robotic limb. Both F^d and F^r are recorded in the test. As Fig. 8 shows, the F^r curve can follow the F^d, indicating that the force control method can output target forces. The control method is implemented on an MCU (STM32F103ZET6) at 100 Hz, using Can bus to communicate with two motor controllers. Outputs of the force sensor (Futek, LCM300, FSH03885) are sampled at the same frequency with the A/D module of MCU. The performance will be improved if we increase the control frequency. As an initial verification of the function, it is enough in the current stage.

4.2 Walking Test of SuperLimbs. To verify the function of the gait control method, the walking test of the SuperLimbs is carried out. Photos of a participant walking with the SuperLimbs on a smooth terrain are shown in Fig. 9. By the coordination of the hip joint, the knee joint, and the prismatic joint, each robotic limb can follow the participant's gait as well as support the load

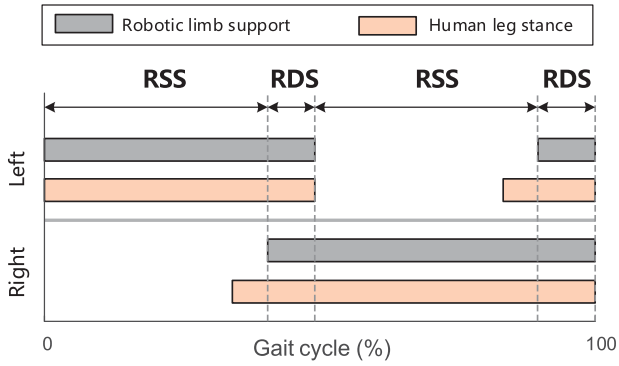

Fig. 6 Phases of the SuperLimbs in a gait cycle. In the RDS (robotic double support) phase, both robotic limbs work in the robotic-limb-support mode to distribute the load weight borne by the human. In the RSS (robotic single support) phase, one robotic limb is in the robotic-limb-swing or the touch-down mode, and the load weight is distributed by the other robotic limb.

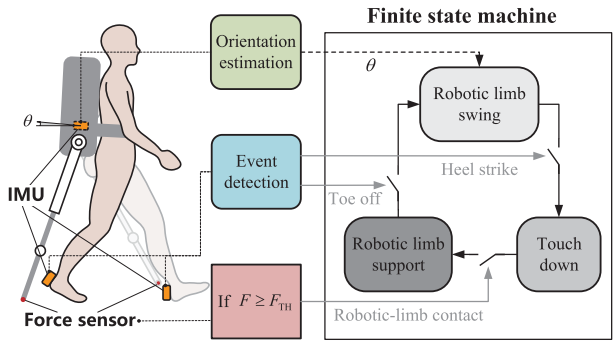

Fig. 7 Diagram of the sensory control. The mode of the robotic limb is driven by the events heel-strike, toe-off, and robotic-limb-contact, detected by the IMUs and the force sensors, respectively. In the robotic-limb-swing mode, the pitch angle of the backpack is estimated to compensate for the error from the body sway.

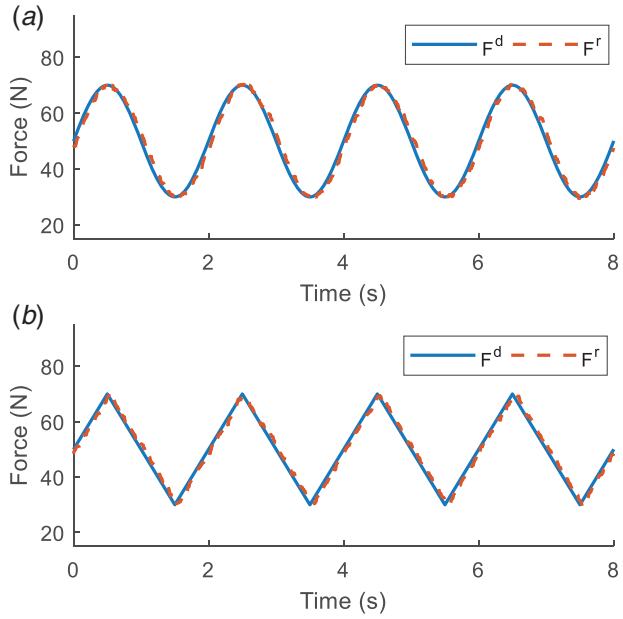

Fig. 8 Results of the force control test on the prismatic joint: (*a*) sinusoid test and (*b*) triangle test. F^d is the desired force in sinusoid or triangle form. F^r is the real force measured by the force sensor.

carriage. The load weight is set to 150 N, and the force amplitude of robotic limb is set to 75 N.

Figure 10(*a*) presents the trajectories of the prismatic joint (x_p) and the hip joint in the flex/extension DOF(θ_{hip}). The robotic-limb-swing mode has two steps. In Step I, the robotic limb swings forward to the next stride. Joint trajectories are formulated by the cubic spline interpolation. After arriving at the target configuration, the robotic limb maintains the pose to wait for the heel-strike of the human leg (Step II). In the touch-down mode, the robotic limb swings backward and extends its length, touching the ground actively. In the robotic-limb-support mode, the hip joint is in zero-torque mode, and the force control is used on the prismatic joint to support the load. Both joints follow the movement of the human participant to avoid constraining the human motions.

Figure 10(*b*) shows the mechanical power of the prismatic joint in a gait cycle. As most of the load weight is borne by the prismatic joint, the main power consumption is cost on this joint. The mechanical power is calculated by $P = F^r v_p$, where F^r is measured by the force sensor at the end of robotic limb, and v_p is the velocity of prismatic joint, calculated by the encoder of motor. The average mechanical power during the robotic-limb-support mode is 4.07 W.

4.3 Load Weight Comparison. To prove the concept of using the SuperLimbs on loaded walking assistance, the participant walked on a smooth terrain in a certain walking speed under three conditions:

(a) walking with the SuperLimbs carrying the load (SuperLimb);
(b) walking with the backpack carrying the load (backpack);
(c) normal walking without the load (unload).

In the SuperLimb condition, the diagram of the experiment measurement is shown in Fig. 11. The human user walked with the load carriage, and the SuperLimbs followed the human gait to distribute the weight borne by the user. The load force between the human participant and the SuperLimbs was measured by a force sensor, to evaluate the weight borne by the participant. The outputs of the force sensor at the end of each robotic limb were also recorded. Insole forces were measured by the pressure insoles (Pedar-X system, Novel, Germany) to estimate the vertical Ground Reaction

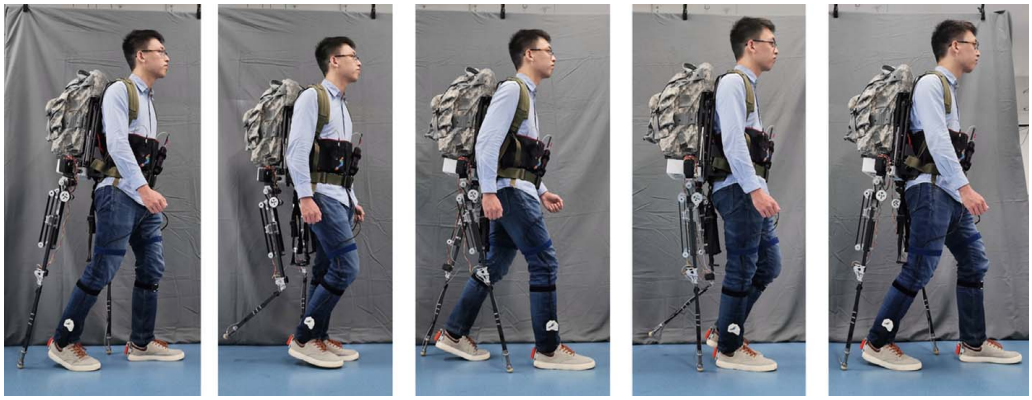

Fig. 9 Photos of a gait cycle of the participant walking with the SuperLimbs

Force (GRF) of the human participant. In the backpack condition, the load force and insole forces were recorded as comparisons. In the unload condition, insole forces were recorded. The participant walked on a pathway back and forth to record about 50 strides under each condition. The walking frequency was set to 0.5 Hz with a metronome to control the walking speed. The average walking speed was approximately 0.7 m/s. The load weight was set to 150 N in both the SuperLimb and the backpack conditions.

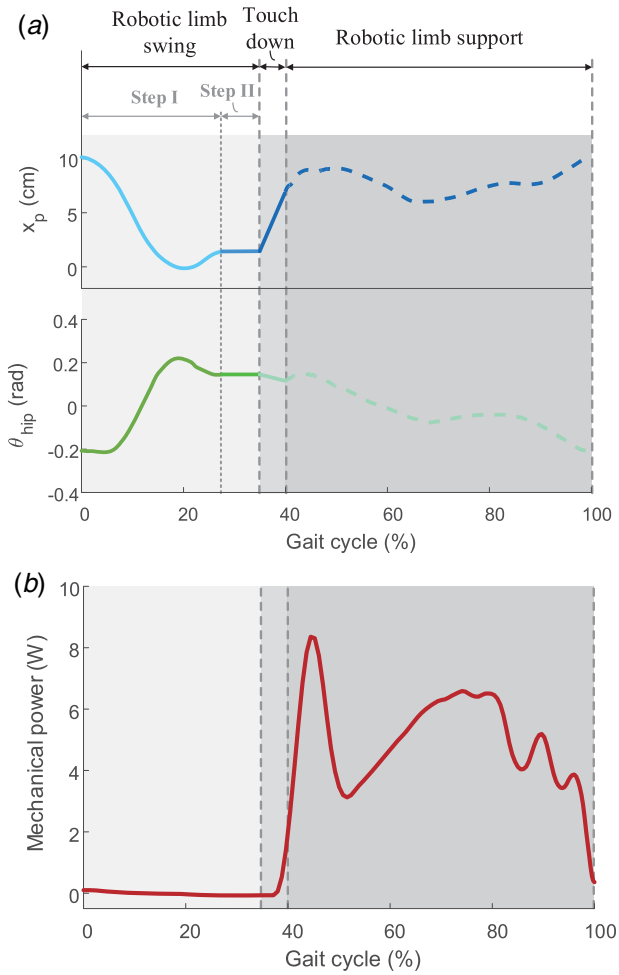

Fig. 10 Joint motions in a gait cycle: (*a*) joint trajectories. The displacement of the prismatic joint (x_p) and the angle of hip joint in the flex/extension DOF (θ_{hip}) are plotted. (*b*) Mechanical power of prismatic joint.

Figure 12 shows the force result in a gait cycle. All data are low-pass filtered by applying a second-order Butterworth filter at a cutoff frequency of 6 Hz. The dashed line is the load force result of the backpack condition for comparison. At any time of the gait cycle, the curve of the SuperLimbs is under the curve of the backpack, indicating that the SuperLimbs can reduce the load force borne by the participant. In the robotic double support (RDS) phase, both robotic limbs are in robotic-limb-support mode to support the load. In the robotic single support (RSS) phase, only one robotic limb supports the load weight, and the other limb is off the ground.

Statistics of measurements under different conditions are shown in Fig. 13. Insole forces of human legs are calculated by adding outputs of the pressure insoles, as Fig. 13(*a*) shows. Figure 13(*b*) describes the statistics of insole forces under three conditions. Means and maximums of insole forces in each stride are calculated. The comparison of the backpack and the unload result indicates that the load weight increases the insole force. The insole force of the

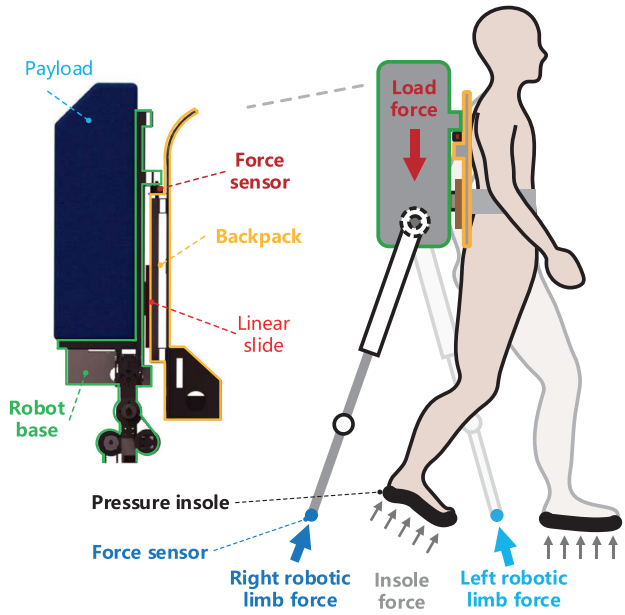

Fig. 11 Diagram of experiment measurements. The participant walks carrying the load with the assistance of the SuperLimbs. The load force, the forces of robotic limbs, and the insole forces are recorded. The load force is measured by the force sensor fixed in the SuperLimb base, which allows measuring the weight borne by the human. The insole forces are measured by the pressure insole, which estimates the vertical GRF of the participant.

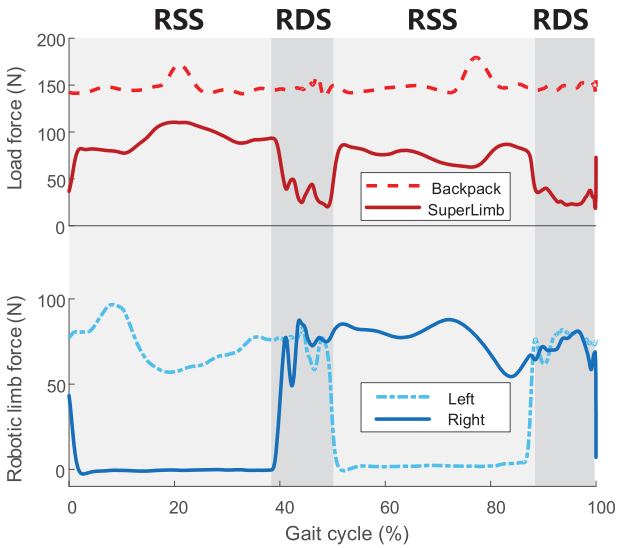

Fig. 12 Force results of the SuperLimbs in a gait cycle. The dashed line is the load force result of the backpack for comparison. In any time of the gait cycle, the curve of SuperLimbs is under the curve of backpack, showing that the SuperLimbs can reduce the load force borne by the participant. In the RDS (robotic double support) phase, both robotic limbs are in robotic-limb-support mode to support the load. In the RSS (robotic single support) phase, only one robotic limb supports the load weight and the other limb is off the ground.

SuperLimb condition is less than the backpack condition, indicating that the SuperLimbs can reduce the load weight borne by the human participant. The increment is reduced by 85.7% on the mean and is reduced by 83.8% on the maximum.

Figure 13(*c*) shows statistics of load forces under the SuperLimb or backpack condition. Compared with the backpack, the load force is reduced by 85.7% in the RDS phase and decreases by 47.0% in the RSS phase. The average decrease of the load force is 55.8%, indicating that the SuperLimbs can reduce the load weight borne by the human participant. The performance can be further optimized by increasing the amplitude of the output force. In this study, the output force of each robotic limb is in constant form for simplicity, so the amplitude is set to 75 N (the half of the load weight) to avoid over supporting in the RDS phase.

In this section, we test the force control of the prismatic joint and the gait control method to verify the function of the SuperLimbs. The concept of SuperLimb assistance is proved by the initial proof experiments under different conditions. Results indicate that the SuperLimbs can follow the human walking as well as reduce the load weight borne by the user. The load force is reduced by 55.8% on average and 85.7% in the RDS phase compared with the backpack. The insole force estimated by the pressure insoles is also reduced with the assistance of the SuperLimb system.

5 Discussion

In this paper, a SuperLimb system to assist human walking with load carriage is proposed. The system is designed to distribute the load weight borne by the human user by transferring the weight to the ground during the human walking. The mechanical design and the gait control of the SuperLimbs are discussed. Functions of the gait control method are verified by experimental tests. Walking experiments are conducted to provide an initial proof of this concept. Results show that the SuperLimbs can distribute 85.7% load weight borne by the human, when both robotic limbs support, and 55.8% load weight on average. This study may inspire the design of other wearable robots and may provide efficient solutions for human loaded walking.

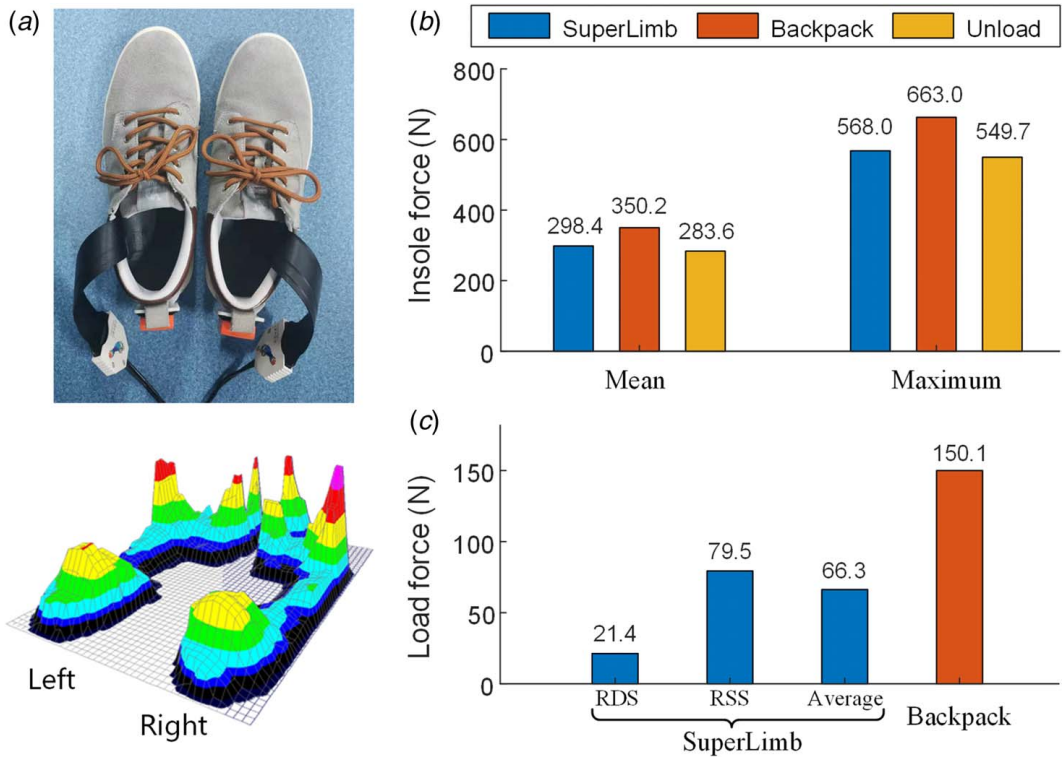

Fig. 13 Experiment results under different conditions. (*a*) Calculation of insole forces. (*b*) Insole force results. Means and maximums of insole forces in each stride are calculated. (*c*) Load force results. Means of load forces in RDS (robotic double support) phases, RSS (robotic single support) phases, and the average are calculated, which are all less than the backpack.

In this study, we only test the SuperLimbs at one walking speed on a smooth terrain as an initial proof of the concept. Our next step is the further study of the performance range, including different walking speeds, different smoothness of terrain, other road conditions, and other locomotion. For other road conditions such as slope and stairs, a vision system is needed for predictive control [31,32]. For other locomotions such as running, we will improve the mechanical system and control method to ensure that the SuperLimbs have enough speed to follow the locomotion.

In this study, the output force of each robotic limb is set to constant form for simplicity, and the amplitude is set to half of the load weight to avoid over supporting. The load weight borne by the human user would be further reduced, if the force amplitude increased. For example, the force amplitude should be set to the load weight in the RSS phase and should be changed into half of the weight in the RDS phase. In our future work, we would optimize the force form and the sensory control method to further improve the performance.

Different from exoskeletons, structures of SuperLimbs are kinematically independent of the human limbs, which can avoid physical interference. Besides exoskeletons and SuperLimbs, many elastically suspended backpacks were also used in loaded walking by regulating the connection between the user and the load carriage [33–37]. This idea may be applied in the SuperLimbs to further improve the assistance performance. The SuperLimbs can reduce the average weight borne by the human user, and the elastically suspended backpacks can change the weight distribution over the gait cycle [37]. Combinations with other wearable robots (e.g., joint-level exoskeletons and soft-suit exoskeletons) may also lead to efficient solutions in loaded walking in a specific environment. Totally speaking, this study has provided a novel solution for loaded walking or other relative situations and can be combined with other wearable robots or equipment easily.

Acknowledgment

This work was supported by the National Key R&D Program of China [Grant 2018YFB1305400 and 2018YFC2001601]; National Natural Science Foundation of China [Grant U1913205, 61533004 and U1613206]; Shenzhen and Hong Kong Innovation Circle Project [Grant SGLH20180619172011638]; and Centers for Mechanical Engineering Research and Education at MIT and SUSTech.

Data Availability Statement

The datasets generated and supporting the findings of this paper are obtainable from the corresponding author upon reasonable request. The authors attest that all data for this study are included in the paper. Data provided by a third party are listed in Acknowledgments. No data, models, or code were generated or used for this paper.

References

[1] Louhevaara, V., Smolander, J., Tuomi, T., Korhonen, O., and Jaakkola, J., 1985, "Effects of an SCBA on Breathing Pattern, Gas Exchange, and Heart Rate During Exercise," J. Occupational Med., **27**(3), pp. 213–216.
[2] Walsh, C. J., Endo, K., and Herr, H., 2007, "A Quasi-Passive Leg Exoskeleton for Load-Carrying Augmentation," Int. J. Human. Rob., **4**(03), pp. 487–506.
[3] Zoss, A. B., Kazerooni, H., and Chu, A., 2006, "Biomechanical Design of the Berkeley Lower Extremity Exoskeleton (BLEEX)," IEEE/ASME Trans. Mechatron., **11**(2), pp. 128–138.
[4] Kazerooni, H., Steger, R., and Huang, L., 2006, "Hybrid Control of the Berkeley Lower Extremity Exoskeleton (BLEEX)," Int. J. Rob. Res., **25**(5–6), pp. 561–573.
[5] Mooney, L. M., Rouse, E. J., and Herr, H. M., 2014, "Autonomous Exoskeleton Reduces Metabolic Cost of Human Walking During Load Carriage," J. Neuroeng. Rehab., **11**(1), p. 80.
[6] Panizzolo, F. A., Galiana, I., Asbeck, A. T., Siviy, C., Schmidt, K., Holt, K. G., and Walsh, C. J., 2016, "A Biologically-Inspired Multi-Joint Soft Exosuit That Can Reduce the Energy Cost of Loaded Walking," J. Neuroeng. Rehab., **13**(1), p. 43.
[7] Mooney, L. M., and Herr, H. M., 2016, "Biomechanical Walking Mechanisms Underlying the Metabolic Reduction Caused by an Autonomous Exoskeleton," J. Neuroeng. Rehab., **13**(4), pp. 1–12.
[8] Gregorczyk, K. N., Hasselquist, L., Schiffman, J. M., Bensel, C. K., Obusek, J. P., and Gutekunst, D. J., 2010, "Effects of a Lower-Body Exoskeleton Device on Metabolic Cost and Gait Biomechanics During Load Carriage," Ergonomics, **53**(10), pp. 1263–1275.
[9] Mooney, L. M., Rouse, E. J., and Herr, H. M., 2014, "Autonomous Exoskeleton Reduces Metabolic Cost of Human Walking," J. Neuroeng. Rehab., **11**(1), p. 80.
[10] Liu, J., Xiong, C., and Fu, C., 2019, "An Ankle Exoskeleton Using a Lightweight Motor to Create High Power Assistance for Push-Off," ASME J. Mech. Rob., **11**(4), p. 041001.
[11] Chang, Y., Wang, W., and Fu, C., 2020, "A Lower Limb Exoskeleton Recycling Energy From Knee and Ankle Joints to Assist Push-Off," ASME J. Mech. Rob., **12**(5), p. 051011.
[12] Hussain, I., Salvietti, G., Spagnoletti, G., Malvezzi, M., Cioncoloni, D., Rossi, S., and Prattichizzo, D., 2017, "A Soft Supernumerary Robotic Finger and Mobile Arm Support for Grasping Compensation and Hemiparetic Upper Limb Rehabilitation," Rob. Auton. Syst., **93**, pp. 1–12.
[13] Tiziani, L., Hart, A., Cahoon, T., Wu, F., Asada, H. H., and Hammond, F. L., 2017, "Empirical Characterization of Modular Variable Stiffness Inflatable Structures for Supernumerary Grasp-Assist Devices," Int. J. Rob. Res., **36**(13–14), pp. 1391–1413.
[14] Llorens-Bonilla, B., Parietti, F., and Asada, H., 2012, "Demonstration-Based Control of Supernumerary Robotic Limbs," 2012 IEEE/RSJ International Conference on Intelligent Robots and Systems (IROS), Vilamoura, Algarve, Portugal, Oct. 7–12, IEEE.
[15] Davenport, C., Parietti, F., and Asada, H. H., 2012, "Design and Biomechanical Analysis of Supernumerary Robotic Limbs," ASME 2012 5th Annual Dynamic Systems and Control Conference Joint With the JSME 2012 11th Motion and Vibration Conference, Fort Lauderdale, FL, Oct. 17–19, American Society of Mechanical Engineers Digital Collection, pp. 787–793.
[16] Bonilla, B. L., and Asada, H. H., 2014, "A Robot on the Shoulder: Coordinated Human-Wearable Robot Control Using Coloured Petri Nets and Partial Least Squares Predictions," 2014 IEEE International Conference on Robotics and Automation (ICRA), Hong Kong, China, May 31–June 7, IEEE, pp. 119–125.
[17] Parietti, F., and Asada, H. H., 2013, "Dynamic Analysis and State Estimation for Wearable Robotic Limbs Subject to Human-Induced Disturbances," 2013 IEEE International Conference on Robotics and Automation (ICRA), Karlsruhe, Germany, May 6–10, IEEE, pp. 3880–3887.
[18] Parietti, F., Chan, K., and Asada, H. H., 2014, "Bracing the Human Body With Supernumerary Robotic Limbs for Physical Assistance and Load Reduction," 2014 IEEE International Conference on Robotics and Automation (ICRA), Hong Kong, China, May 31–June 7, IEEE, pp. 141–148.
[19] Parietti, F., and Asada, H. H., 2014, "Supernumerary Robotic Limbs for Aircraft Fuselage Assembly: Body Stabilization and Guidance by Bracing," 2014 IEEE International Conference on Robotics and Automation (ICRA), Hong Kong, China, May 31–June 7, IEEE,pp. 1176–1183.
[20] Kurek, D. A., and Asada, H. H., 2017, "The Mantisbot: Design and Impedance Control of Supernumerary Robotic Limbs for Near-Ground Work," 2017 IEEE International Conference on Robotics and Automation (ICRA), Singapore, May 29–June 3, IEEE,pp. 5942–5947.
[21] Parietti, F., Chan, K. C., Hunter, B., and Asada, H. H., 2015, "Design and Control of Supernumerary Robotic Limbs for Balance Augmentation," 2015 IEEE International Conference on Robotics and Automation (ICRA), Seattle, WA, May 26–30, IEEE, pp. 5010–5017.
[22] Parietti, F., and Asada, H., 2016, "Supernumerary Robotic Limbs for Human Body Support," IEEE Trans. Rob., **32**(2), pp. 301–311.
[23] Treers, L., Lo, R., Cheung, M., Guy, A., Guggenheim, J., Parietti, F., and Asada, H., 2016, "Design and Control of Lightweight Supernumerary Robotic Limbs for Sitting/Standing Assistance," International Symposium on Experimental Robotics, Tokyo, Japan, Oct. 3–6, Springer, pp. 299–308.
[24] Gonzalez, D. J., and Asada, H. H., 2018, "Design of Extra Robotic Legs for Augmenting Human Payload Capabilities by Exploiting Singularity and Torque Redistribution," 2018 IEEE/RSJ International Conference on Intelligent Robots and Systems (IROS), Madrid, Spain, Oct. 1–5, IEEE, pp. 4348–4354.
[25] Gonzalez, D. J., and Asada, H. H., 2019, "Hybrid Open-Loop Closed-Loop Control of Coupled Human–Robot Balance During Assisted Stance Transition With Extra Robotic Legs," IEEE Rob. Autom. Lett., **4**(2), pp. 1676–1683.
[26] Parietti, F., and Asada, H. H., 2017, "Independent, Voluntary Control of Extra Robotic Limbs," 2017 IEEE International Conference on Robotics and Automation (ICRA), Singapore, May 29–June 3, IEEE, pp. 5954–5961.
[27] Penaloza, C. I., and Nishio, S., 2018, "BMI Control of a Third Arm for Multitasking," Sci. Rob., **3**(20), p. eaat1228.
[28] Chen, G., Chan, C. K., Guo, Z., and Yu, H., 2013, "A Review of Lower Extremity Assistive Robotic Exoskeletons in Rehabilitation Therapy," Crit. Rev. Biomed. Eng., **41**(4–5), pp. 343–363.
[29] Hao, M., Chen, K., and Fu, C., 2019, "Effects of Hip Torque During Step-to-Step Transition on Center-of-Mass Dynamics During Human Walking Examined With Numerical Simulation," J. Biomech., **90**, pp. 33–39.
[30] Hao, M., Chen, K., and Fu, C., 2019, "Smoother-Based 3D Foot Trajectory Estimation Using Inertial Sensors," IEEE Trans. Biomed. Eng., **66**(12), pp. 3534–3542.

[31] Zhang, K., Xiong, C., Zhang, W., Liu, H., Lai, D., Rong, Y., and Fu, C., 2019, "Environmental Features Recognition for Lower Limb Prostheses Toward Predictive Walking," IEEE Trans. Neural Syst. Rehab. Eng., **27**(3), pp. 465–476.
[32] Zhang, K., Luo, J., Xiao, W., Zhang, W., Liu, H., Zhu, J., Lu, Z., Rong, Y., de Silva, C. W., and Fu, C., 2020, "A Subvision System for Enhancing the Environmental Adaptability of the Powered Transfemoral Prosthesis," IEEE Trans. Cybernet., **PP**(99), pp. 1–13.
[33] Wu, Y., Chen, K., and Fu, C., 2016, "Effects of Load Connection Form on Efficiency and Kinetics of Biped Walking," ASME J. Mech. Rob., **8**(6), p. 061015.
[34] Yang, L., Zhang, J., Xu, Y., Chen, K., and Fu, C., 2020, "Energy Performance Analysis of a Suspended Backpack With An Optimally Controlled Variable Damper for Human Load Carriage," Mech. Mach. Theory, **146**, p. 103738.
[35] Rome, L. C., Flynn, L., Goldman, E. M., and Yoo, T. D., 2005, "Generating Electricity While Walking With Loads," Science, **309**(5741), pp. 1725–1728.
[36] Rome, L. C., Flynn, L., and Yoo, T. D., 2006, "Biomechanics: Rubber Bands Reduce the Cost of Carrying Loads," Nature, **444**(7122), p. 1023.
[37] Kuo, A. D., 2005, "Harvesting Energy by Improving the Economy of Human Walking," Science, **309**(5741), pp. 1686–1687.